Nuclear Engineering and Technology 55 (2023) 2474–2482

Contents lists available at ScienceDirect

Nuclear Engineering and Technology

journal homepage: www.elsevier.com/locate/net

Original Article

Multigroup cross-sections generated using Monte-Carlo method with flux-moment homogenization technique for fast reactor analysis

Yiwei Wu [a], Qufei Song [a], Kuaiyuan Feng [a], Jean-François Vidal [b], Hanyang Gu [a], Hui Guo [a, *]

[a] School of Nuclear Science and Engineering, Shanghai Jiao Tong University, Shanghai, China
[b] CEA, DES/IRESNE/DER/SPRC/LEPh, Cadarache, F-13108, Saint-Paul-lez-Durance, France

ARTICLE INFO

Article history:
Received 19 January 2023
Received in revised form
7 April 2023
Accepted 8 April 2023
Available online 10 April 2023

Keywords:
Fast reactor
Monte-Carlo
Multi-group cross-sections
Flux-moment homogenization
Metal fuel

ABSTRACT

The development of fast reactors with complex designs and operation status requires more accurate and effective simulation. The Monte-Carlo method can generate multi-group cross-sections in arbitrary geometry without approximation on resonances treatment and leads to good results in combination with diffusion codes. However, in previous studies, the coupling of Monte-Carlo generated multi-group cross-sections (MC-MGXS) and transport solvers has shown relatively large biases in fast reactor problems. In this paper, the main contribution to the biases is proved to be the neglect of the angle-dependence of the total cross-sections. The flux-moment homogenization technique (MHT) is proposed to take into account this dependence. In this method, the angular dependence is attributed to the transfer cross-sections, keeping an independent form for the total sections. For the MET-1000 benchmark, the multi-group transport simulation results with MC-MGXS generated with MHT are improved by 700 pcm and an additional 120 pcm with higher order scattering. The factors that cause the residual bias are discussed. The core power distribution bias is also significantly reduced when MHT is used. It proves that the MC-MGXS with MHT can be applicable with transport solvers in fast reactor analysis.

1. Introduction

The higher economic and safety standard in Gen-IV reactor development requires advanced reactor designs and accurate neutronic simulation tools. The Monte-Carlo method with pointwise continuous-energy cross-sections (so-called CEMC method) can solve neutron transport problems on complex geometries without major approximation of the resonance self-shielding effect. The two-step deterministic method can be much faster than the CEMC method but at the cost of approximations in space discretization, angle representations, and energy structure. The deterministic codes are widely used for core analysis, especially in design optimization, multiphysics modeling, and complex depletion analysis, relying on homogenized multigroup cross-sections (MGXS).

The advanced reactor designs require accurate simulation of complex geometries and neutron spectrum, which challenge the traditional MGXS generation method. There is a growing interest in generating MGXS using the CEMC method (so-called MC-MGXS). The MC-MGXS is developed in MCNP [1,2], McCARD [3,4], SERPENT [5,6], RMC [7], OpenMC [8], MCS [9], and so on. The MC-MGXS method makes it possible to treat resonance self-shielding and spatial and angular flux variations with an arbitrary level of detail at assembly scale, and to generate homogenized cross-sections for full-core calculations.

The two-step scheme coupling MC-MGXS and diffusion core solver was widely investigated for fast reactor analysis, such as Serpent/DYN3D [10], MCS/RAST [9], Serpent/Griffin [11] and so on. Satisfactory results can therefore be obtained from this method for various numerical and experimental benchmarks of sodium fast reactor (SFR). However, diffusion solvers showed shortcomings in regions with drastic flux change and strong scattering anisotropy. This deficiency can be improved by certain correction techniques such as the “Superhomogenization” equivalence (SPH).

The two-step scheme coupling MC-MGXS and transport core solver was also investigated, such as Serpent/VARIANT [12], MCS-MCS [9], OpenMC/OpenMC [13]. The coupling of MC-MGXS with the simplified spherical harmonics (SPN) solver showed a 643 pcm overestimation in 2D metallic SFR [12]. The coupling of MC-MGXS

* Corresponding author.
E-mail address: hui.guo@sjtu.edu.cn (H. Guo).

https://doi.org/10.1016/j.net.2023.04.011

with MC MG transport solver showed a 1085 pcm [9] in the MET-1000 benchmark. These assessments show that there is a large overestimation of core reactivity in the MC-MGXS/transport scheme for fast reactor analysis.

The objective of this paper is to investigate the cause of the overestimation of the MC-MGXS/transport scheme in the SFR analysis and to propose a flux-moment homogenization method in the generation of MGXS using Monte-Carlo to reduce this overestimation.

The paper structure is the following.

- in section 2, the standard MC-MGXS method, the benchmark case, the decomposition of the overestimation, and the flux-moment homogenization method will be presented,
- in section 3, the results with flux-moment homogenization are discussed,
- the summary and conclusion constitute Section 4.

2. Methods

2.1. Scalar flux homogenization

For the MC-MGXS method in this work, the Monte-Carlo code OpenMC [14] is used to generate MGXS. The OpenMC code generates MGXS by tallying reaction rates and scalar flux in the specified space and energy groups. For reaction cross-sections like total (Σ_t), absorption (Σ_a), and fission production ($\nu\Sigma_f$), the cross-sections are calculated as:

$$\Sigma_{k,x}^{G} = \frac{\int_k dr \int_G \Sigma_x(r,E)\phi(r,E)dE}{\int_k dr \int_G \phi(r,E)dE} = \frac{R_{k,x}^{G}}{\phi_k^{G}} \tag{1}$$

Where $\Sigma_{k,x}^{G}$ is the homogenized cross-section for the x-type reaction in energy group G and region r, $R_{k,x}^{G}$ is the x-type reaction rate in group G and region r and ϕ_k^{G} is the corresponding scalar flux.

For the scattering production term, the outgoing energy needs to be considered. The transfer matrix is calculated as:

$$\Sigma_{k,s,\ell}^{G'\to G} = \frac{\int_k dr \int_G dE \int_{G'} \Sigma_{s,\ell}(r,E'\to E)\phi(r,E')dE'}{\int_k dr \int_{G'} \phi(E)dE} = \frac{R_{k,s,\ell}^{G'\to G}}{\phi_k^{G'}} \tag{2}$$

where $\Sigma_{k,s,l}^{G'\to G}$ is the order-L transfer section from energy group G' to G, $\Sigma_{s,\ell}$ is the order-l scattering section, Other multigroup parameters like multiplicity and fission spectrum are generated following reference [8] formula.

Note that the previous definition uses scalar flux to weight and generate MGXS. OpenMC can also provide MGXS in an range ω of polar or azimuthal angles in an explicit way:

$$\tilde{\Sigma}_{k,x,\omega}^{G} = \frac{\int_k dr \int_\omega d\Omega \int_G \Sigma_x(r,E)\psi(r,E,\Omega)dE}{\int_k dr \int_\omega d\Omega \int_G \psi(r,E,\Omega)dE} \tag{3}$$

In the following, AiPj is used to indicate that the incident angle is discretized into i azimuthal sections and j polar sections, thus having a total number of i × j directions. For instance, the A1P1 is the option without angle discretization, which is widely used in most multigroup core solvers, while the A16P12 represents a 192-angle discretization which can be generated and used in OpenMC. Reference [15] suggests that the angle-dependence of MGXS may influence the transport simulation result, in particular for regions near strong absorbers or including different materials. The angle-dependent MGXS can be used directly in the MC MG transport mode in OpenMC to investigate the effect of angle-dependent MGXS. However, the angle-dependent MGXS is not easily compatible with deterministic core solvers.

It must be noticed that the elements of the high-order transfer matrices should be rigorously generated by weighting by the flux Legendre moment as:

$$\tilde{\Sigma}_{k,s,\ell}^{G'\to G} = \frac{\int_k dr \int_G dE \int_{G'} \Sigma_{s,l}(r,E'\to E)\phi_\ell(r,E')dE'}{\int_k dr \int_{G'} \phi_l(r,E)dE} \tag{4}$$

where ϕ_ℓ is the Legendre moment of neutron flux. However, it is not possible for MC codes to tally the integral value of point cross-sections and flux Legendre moment for the moment, so the high-order transfer matrices are generated with scalar flux weighted as Eq. (2). The approximation leads to inaccurate high-order transfer matrices in core simulations.

2.2. Benchmark description

The metallic SFR MET-1000 is used as a verification benchmark [16]. As shown in Fig. 1, the benchmark core consists of 72 inner fuel, 102 outer fuel, and 114 reflector assemblies, 66 radial shielding assemblies, and 19 control rod assemblies.

In the MGXS generation step, the MGXS of the different regions of the core are generated from a 3D whole-core heterogeneous simulation with the continuous-energy Monte-Carlo method, with 100 inactive batches, 400 active batches, and 5 billion of particles per batch. This MGXS generation method excludes the influence of unrealistic boundary conditions and ensure that MGXS have been homogenized by the real spectrum. The 24-group energy structure used is derived from the ECCO-33G structure [17] by grouping the last 10 groups into one because of the low level of the thermal flux [18].

In the core calculation step, the multigroup simulation capability in OpenMC is used. The MC MG transport method follows the same principle as the CEMC method but with MGXS generated from the previous step. The MC MG transport method can solve transport problems with homogenous (see Fig. 2) or heterogeneous cores. Moreover, the MC MG transport solver in OpenMC is compatible with the angle-dependent MGXS.

Our results show that the MC-MGXS/MC MG transport scheme overestimates the reactivity by 1192 pcm. Faced with such a large bias, the accuracy of the MGXS must be verified.

2.3. Influence of angle-dependence

One possible reason that leads to this large bias is that the angle-dependence of MGXS is neglected; another is the inaccuracy of high-order scattering matrices. The two possible reasons are both mentioned in Section 2.1. The influence of inaccurate high-order scattering matrices can hardly be quantified directly, but the influence of angle-dependence of MGXS can be evaluated by

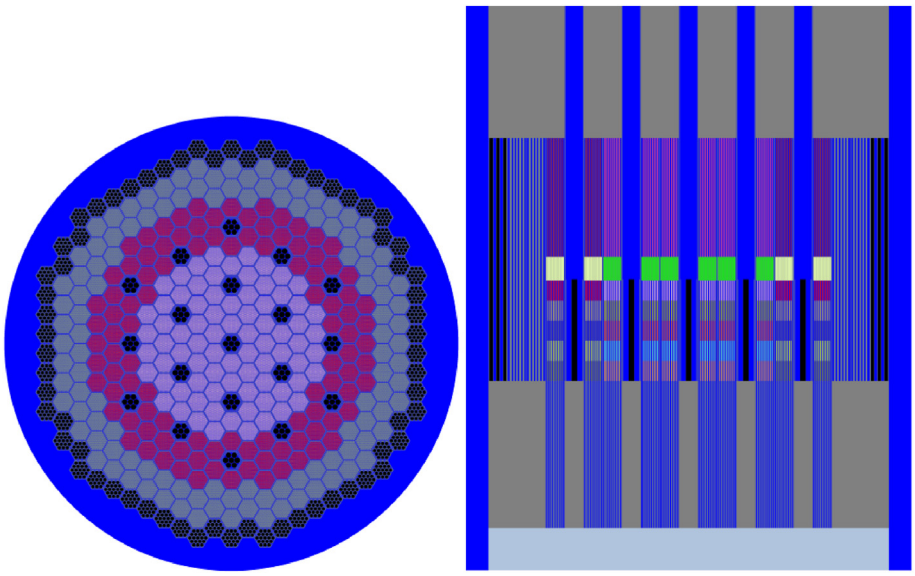

Fig. 1. MET-1000 heterogeneous model in OpenMC (left: radial; right: axial).

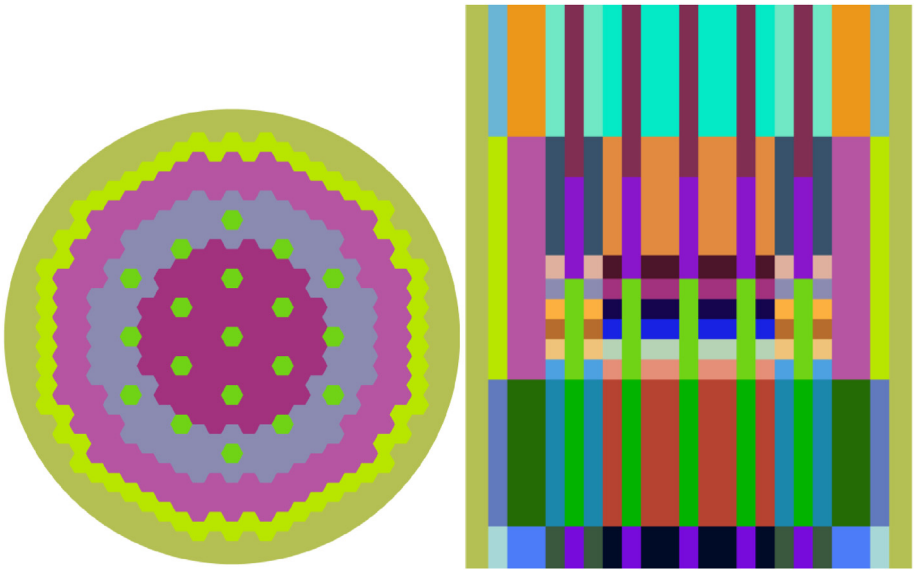

Fig. 2. MET-1000 homogeneous model in OpenMC (left: radial; right: axial).

generating angle-dependent MGXS for the incident angle discretization.

However, the discretization also changes the high-order scattering matrices in MGXS and changes the influence of unprecise high-order scattering matrices. To eliminate this influence, the isotropic-in-lab (IIL) case is simulated in this paper beside the reference anisotropic-in-lab (AIL) case. The IIL means that elastic scattering is isotropic in the laboratory frame. The IIL case wrongly estimates the core parameters in CEMC calculation, while it only requires zero-order scatter matrices in MC MG transport calculation. Results of IIL problems can suggest the order of magnitude of the influence of the angle dependence.

The results with angle-dependent MGXS are shown in Table 1. When A8P4 discretization is used in the AIL case, the overestimation in core reactivity is reduced by 707 pcm. When increasing the angular discretization, the overestimation is further reduced but the improvement seems to converge. The A16P12 discretization reduces the overestimation by 772 pcm. The results with angle discretization in the IIL system are also computed, the A16P12 result of IIL problem also reduces the overestimation by 638 pcm compared to the 938 pcm obtained with A1P1. The analysis of the IIL results suggests that the influence of angle-dependent MGXS contributes more than two-thirds of the total difference and is the main element that causes the MG simulation bias; the influence of unprecise high-order scattering matrices is thus limited.

The influence of the angle dependence of different cross-section types is shown in Table 2. The angle discretization is set as A16P12. The MGXS with angle-dependent Σ_t shows only a 6 pcm bias compared to the case with all angle-dependent cross-sections. Moreover, angle-dependent Σ_a or angle-dependent $\Sigma_{s,l}$ do not show obvious optimization. It suggests that the overestimation in reactivity is mainly due to the neglect of angle dependence in Σ_t.

Even though angle-dependent cross-sections such as A16P12

Table 1
k_{eff} using MGXS with different angle discretization.

Scattering	Core solver	Angle discretization	k_{eff}	$\Delta\rho_{MG-CE}$ (pcm)
Anisotropic	CE		1.02898 ± 0.00004	–
	MG	A1P1	1.04176 ± 0.00003	1192 ± 5
		A8P4	1.03414 ± 0.00003	485 ± 5
		A16P4	1.03407 ± 0.00003	478 ± 5
		A16P8	1.03349 ± 0.00003	424 ± 5
		A16P12	1.03345 ± 0.00003	420 ± 5
Isotropic	CE		1.06578 ± 0.00004	–
	MG	A1P1	1.07654 ± 0.00003	938 ± 5
		A8P4	1.06982 ± 0.00003	354 ± 5
		A16P4	1.06972 ± 0.00003	346 ± 5
		A16P8	1.06937 ± 0.00003	315 ± 5
		A16P12	1.06920 ± 0.00003	300 ± 5

Table 2
k_{eff} using MGXS with different angle-dependent cross-section types.

Core solver	Angle-dependence	k_{eff}	Δρ (pcm)
CE		1.02898 ± 0.00004	–
MG	None	1.04176 ± 0.00003	1192 ± 5
	Σ_t	1.03351 ± 0.00003	426 ± 5
	Σ_t & Σ_a	1.03365 ± 0.00003	440 ± 5
	Σ_t & $\Sigma_{s,l}$	1.03354 ± 0.00003	429 ± 5
	All	1.03345 ± 0.00003	420 ± 5

can reduce the bias in MG calculation, they require larger data sizes, needs more memory in simulation, and their applicability is limited. Moreover, they are not compatible with widely used deterministic core solvers. Therefore, novel techniques should be introduced in commonly used formatting, e.g. A1P1, to cover angular dependency while keeping generality.

2.4. Flux-moment homogenization technique

In most deterministic transport codes, MGXS are independent of the incident angle. In Ref. [19] and Reference [20], the 'consistent-P' approximation [21] is generalized to 2D and 3D for fast reactor analysis, and called flux-moment homogenization technique (MHT).

The flux-moment homogenization is based on neutron conservation. The stationary Boltzmann neutron transport equation with A1P1 MGXS can be written as:

$$L(r,\Omega)+T(r,\Omega)=S(r,\Omega)+F(r,\Omega)$$

Where the L term means the leakage, the T term means the total reaction rate, the S term means the scattering source, and the F term means the fission term. Developing the angular flux and transfer XS in spherical harmonics $Y_{\ell,m}$ in T and S gives:

$$T=\Sigma^G_{k,t}\psi_k(\Omega)=\sum_{\ell}\frac{2\ell+1}{4\pi}\sum_{m=-l}^{\ell}\Sigma^G_{k,t}\phi^G_{k,\ell,m}Y_{\ell,m}(\Omega) \tag{5}$$

$$S=\sum_{G'}\sum_{\ell}\frac{2l+1}{4\pi}\sum_{m=-\ell}^{\ell}\Sigma^{G'\to G}_{k,s,\ell,m}\phi^{G'}_{k,\ell,m}Y_{\ell,m}(\Omega) \tag{6}$$

However, if the angle dependence of the total cross-sections is considered, the exact equation is:

$$L(r,\Omega)+\tilde{T}(r,\Omega)=S(r,\Omega)+F(r,\Omega) \tag{7}$$

where the angle-dependency is also taken into account by a spherical harmonics expansion:

$$\tilde{T}=\Sigma^G_{k,t}(\Omega)\psi_k(\Omega)=\sum_{\ell}\frac{2\ell+1}{4\pi}\sum_{m=-\ell}^{\ell}\Sigma^G_{k,t,\ell,m}\phi^G_{k,\ell,m}Y_{\ell,m}(\Omega) \tag{8}$$

To keep an isotropic total cross-section in simulation, the T term should be considered on the left side of the equation, leading to:

$$L+T=S+T-\tilde{T}+F \tag{9}$$

Notice that the flux terms in S, T and $\tilde{T}$ are the same and they can be combined:

$$\widehat{S}=S+T-\tilde{T}\#=\sum_{G'}\sum_{\ell}\frac{2\ell+1}{4\pi}\sum_{m=-\ell}^{\ell}\left(\Sigma^{G'\to G}_{k,s,\ell,m}+\delta_{G,G'}\left(\Sigma^G_{k,t}-\Sigma^G_{k,t,\ell,m}\right)\times\right)\phi^G_{k,\ell,m}Y_{\ell,m}(\Omega) \tag{10}$$

Equivalent scattering matrices can be obtained:

$$\widehat{\Sigma}^{G'\to G}_{k,s,\ell,m}=\Sigma^{G'\to G}_{k,s,\ell,m}+\delta_{GG'}\left(\Sigma^G_{k,t}-\Sigma^G_{k,t,\ell,m}\right) \tag{11}$$

In doing so, we have to deal with spherical harmonic moments for the scattering matrices. The dataset form is still complex and with poor generality. To fit the isotropic form of XS data, Vidal et al. proposed in Ref. [13] a collapsing method based on the least square method to collapse spherical harmonic moments into Legendre moments:

$$\widehat{\Sigma}^{G'\to G}_{k,s,\ell}=\Sigma^{G'\to G}_{k,s,\ell}+\delta_{GG'}\left(\Sigma^G_{k,t}-\Sigma^G_{k,t,\ell}\right) \tag{12}$$

where:

$$\Sigma^G_{k,t,\ell}=\frac{\sum_{-\ell}^{\ell}\phi^G_{k,\ell,m}R^G_{k,t,\ell,m}}{\sum_{-\ell}^{\ell}{\phi^G_{k,\ell,m}}^2} \tag{13}$$

where $R^G_{k,t,\ell,m}$ and $\phi^G_{k,\ell,m}$ can be directly tallied in the MC code.

reference [20] refers to numerical divergence when MGXS with MHT is used in the deterministic method. A fix-up is used to set the corrected high-order scattering matrices to no more than zero-order scattering matrices to avoid divergence:

$$if \left|\widehat{\Sigma}_{k,s,\ell}^{G'\to G}\right| > \Sigma_{k,s,0}^{G'\to G}, let\ \widehat{\Sigma}_{k,s,\ell}^{G'\to G} = \Sigma_{k,s,0}^{G'\to G} \bullet \frac{\widehat{\Sigma}_{k,s,\ell}^{G'\to G}}{\left|\widehat{\Sigma}_{k,s,\ell}^{G'\to G}\right|}$$

The MHT changes the angle distribution of the scattering reaction to represent the anisotropy of the total cross-sections. The correction should be appropriate to all transport solvers. The results with MHT homogenization are discussed in the following.

3. Results and discussions

In the verification calculations, there are 100 inactive batches, 400 active batches, and 50 thousand particles per batch in all MC MG simulations. Unless otherwise specified, the maximum scattering order is 3.

3.1. Reactivity

The reactivity results of MG simulations with different MGXS in the benchmark at all control rods out(ARO) are presented in Table 3.The results show that MHT can reduce the initial reactivity bias of 1192 pcm without MHT by 698 pcm. The result with MHT is similar to that with angle-dependent MGXS, but there is still 74 pcm that the MHT can not reduce. 6 pcm of the 74 pcm are due to the influence of angle-dependent XS except Σ_t. The reason that causes the remaining 68 pcm difference is the insufficient expansion order, which will be discussed in detail in Section 3.5.

Results of the benchmark at all control rods inserted(ARI) status are presented in Table 4. Notice that the core at ARI is calculated to obtained control rods worth, the reactivity difference between ARO and ARI configurations corresponds to the control rod worth $\Delta\rho_{CR}$. The MGXS w/o MHT overestimates by 915 pcm the control rod worth, the A16P12 discretization overestimates it by 916 pcm, and the MGXS w/i MHT overestimates it by 992 pcm. The angle-dependent MGXS or MHT does not change the influence of the spatial self-shielding effect of control assemblies during homogenization, or optimized control rod worth estimation.

The overestimation of control rods worth is due to the homogenization and the MGXS generated with whole-core model at ARO, whose cross-sections of control rods are not appliable at ARI. The problem can be solved by SPH method or generating MGXS with core at ARI. But it is not the problem this paper is about.

3.2. Power distribution

The errors on power distribution are shown in Figs. 3 and 4. MG results overestimate the power on peripheral assemblies and underestimate it on central ones. For the ARO configuration, the results with MGXS without MHT show maximum biases of 4.02%/-4.10% radially and 3.03%/-3.63% axially, with a RMSE of 1.54%. MC-MGXS with MHT reduces the biases to 2.76%/-2.39% radially and 0.79%/-2.25% axially, and the RMSE is reduced to 0.76%. For the ARI configuration, the MC-MGXS with MHT also reduced the maximum biases from 7.17%/-5.96% to 5.28%/-3.34% radially and 7.00%/-6.73% to 2.46%/-3.84% axially, and the RMSE is reduced from 3.36% to 1.86%. The global biases are obviously reduced. In both ARO and ARI configurations, the overestimation of peripheral and the underestimation of central assemblies are reduced. These results prove that the MC-MGXS with MHT can effectively compensate for the bias caused by the angle-dependence of Σ_t.

Table 3
Multiplication factor of results with different MGXS.

Status	Cross-sections		k_{eff}	Δρ (pcm)
ARO	CE		1.02898	–
	MG	w/o MHT	1.04176	1192
		A16P12	1.03345	420
		w/i MHT	1.03424	494

a Standard deviation of Reference keff = 0.00004.
b Standard deviation of Reactivity bias = 5 pcm.

Table 4
Control rods worth estimation with different MGXS.

Status	Cross-sections		k_{eff}	$\Delta\rho_{CR}$ (pcm)	$\Delta(\Delta\rho_{CR})$ (pcm)
ARI	CE		0.86632	18247	–
	MG	w/o MHT	0.86841	19162	915
		A16P12	0.86262	19163	916
		w/i MHT	0.86260	19239	992

a Standard deviation of Reference keff = 0.00004.
b Standard deviation of Reactivity bias = 5 pcm.

3.3. Decomposition of MHT improvement

The effect of using angle-dependent MGXS only in different regions is shown in Table 5. The angle-dependent Σ_t in the reflector regions show the largest influence on reactivity prediction: MHT applied on all reflector regions (axial and radial) can reduce the bias in reactivity by 491 pcm. In structure regions, it has also a considerable effect of 311 pcm. Angle-dependent Σ_t in fuel regions affects the result more slightly. Angle-dependence of absorber regions does not influence the ARO reactivity. However, in the case of all control rods are inserted, the angle-dependent effect can be observed: it is 213 pcm in absorber regions. Fuel, reflector and structure regions also contribute to the effect at ARI. The angle-dependent effect of absorber regions can reduce the overestimation of the control rod worth, but it is counterbalanced by the influence of other regions. The mutual interference between the different regions leads to some differences between the global effect and the summation of local effects.

3.4. Multigroup cross-sections

To highlight the obvious effect of reflector regions, the high-order scattering cross-sections of the radial reflector assemblies are shown in Fig. 5. The scattering cross-sections without correction show tiny absolute values in low-energy groups and increase to a relatively large value in high-energy groups. It means that the strong anisotropic effect occurs for high-energy neutrons. With MHT, the scattering XS in low-energy groups show larger absolute values than those in high-energy groups and large differences from those without correction. The largest value appeared for group 19 for the order-2 XS and for group 14 for the order-1 and order-2 XS. In high-energy groups, MHT hardly changes the cross-sections.

The probability density function (PDF) of the scattering emergence angle in the reflector is shown in Fig. 6 for the two groups, 14 and 19. The emergence angle distribution is nearly linear without MHT. Only the order-1 matrix shows an observable influence on the anisotropy effect. In these groups, the G-to-G transfer section with MHT shows a greater difference on the probability for positive cosine than for negative cosine compared to that without correction. It means that neutrons are more likely to go out forward after scattering. This can explain the improvement in the power distribution and reactivity: MHT strengthens the leakage in reflectors, thus the reaction rates in outer assemblies are decreased, the core reactivity overestimation is reduced, and the power distribution better agrees with the reference.

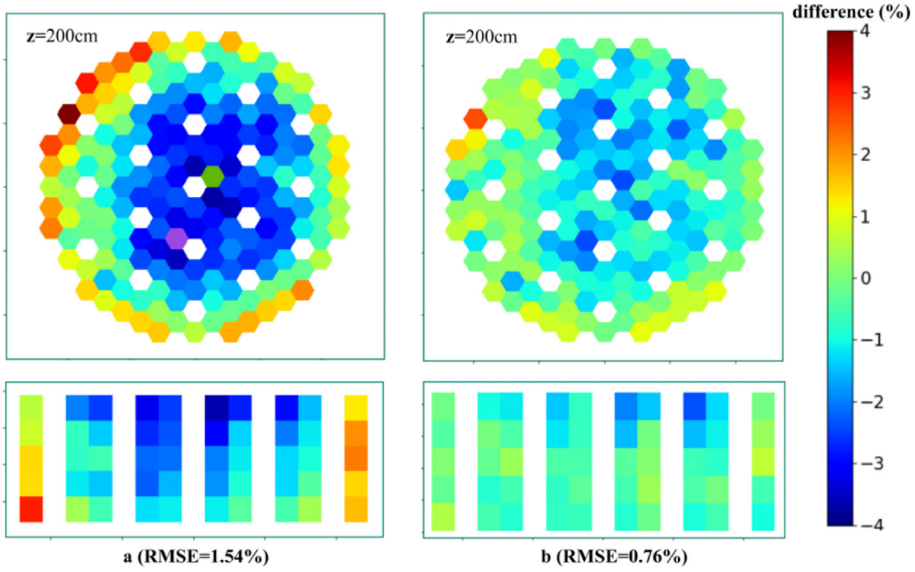

Fig. 3. Power distribution bias at ARO (a: w/o MHT; b: w/i MHT).

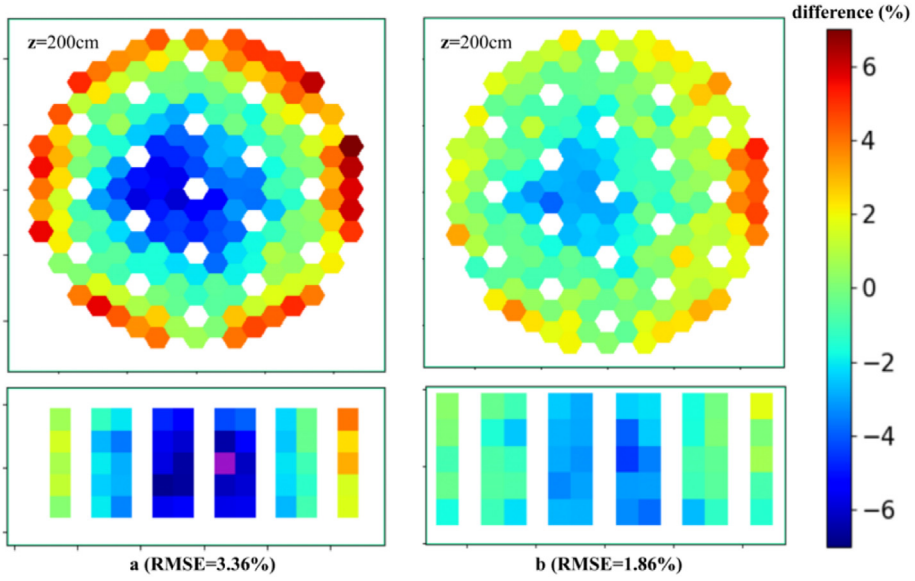

Fig. 4. Core power distribution bias at ARI (a: w/o MHT; b: w/i MHT).

Table 5
Local effect of angle-dependent Σ_t.

Status	ARO		ARI	
	Keff	$\Delta\rho_0$ (pcm)	keff	$\Delta\rho_0$ (pcm)
Reference	1.02898	–	0.86632	–
MG without correction	1.04176	1192	0.86841	278
Corrected region	Keff	$\Delta\rho_0$-$\Delta\rho$ (pcm)	keff	$\Delta\rho_0$-$\Delta\rho$ (pcm)
active fuel	1.04076	92	0.86695	194
reflector	1.03646	491	0.86426	553
shielding	1.04173	3	0.86822	25
structure	1.03840	311	0.86674	222
Absorber	1.04197	−16	0.87002	−213
Summation	–	881	–	781
all	1.03424	698	0.86260	776

a Standard deviation of Reference keff = 0.00004.
b Standard deviation of Reactivity bias = 5 pcm.

3.5. Residual bias

There is still a reactivity bias of 494 pcm after accounting for and compensating for the angle-dependence of the cross-sections. The bias can be broken down as follows.

1) the residual of MHT to the A16P12 method of about 74 pcm,
2) the lack of scattering orders which induces some error in the anisotropic scattering,
3) the spatial and energy homogenization effect,
4) the effect of inaccurate high-order scattering matrices,
5) Other reasons like the interaction of the above factors, and elements that may be neglected in this paper.

Element 1 and element 2 are interacting. The increase of the scattering order not only improves the anisotropic scattering

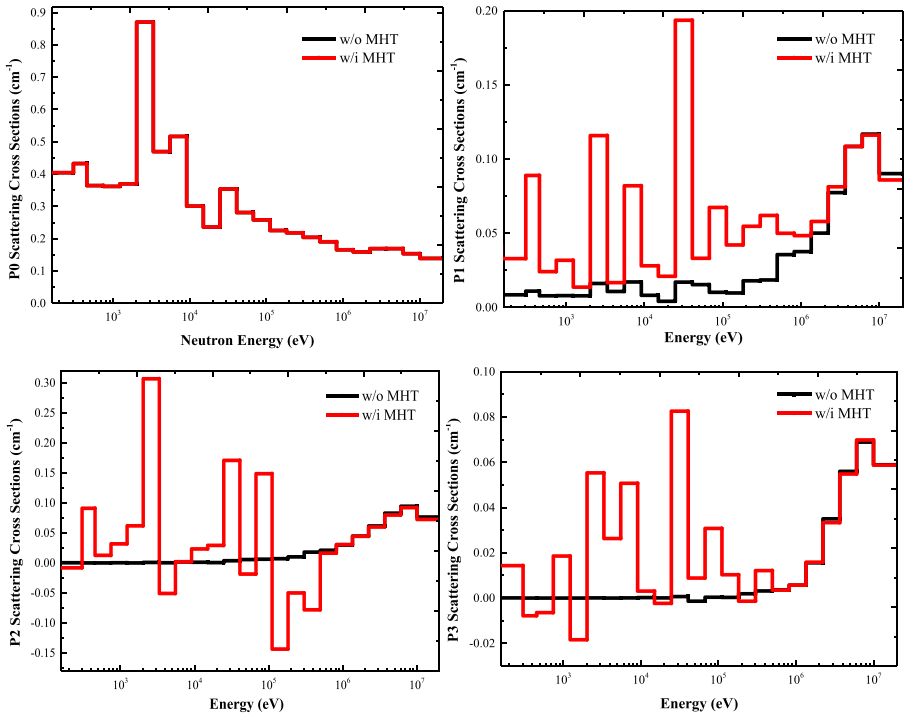

Fig. 5. Multi-group scattering sections of reflector regions.

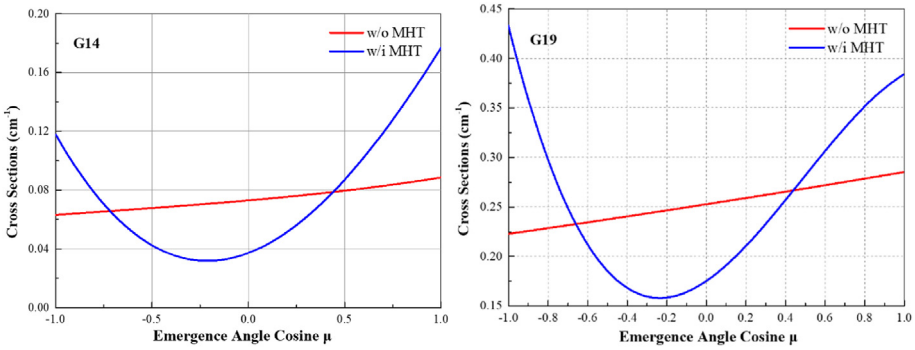

Fig. 6. Angle-dependent transfer sections of the reflector region.

expression but also increases the modification order in MHT. The reactivity results with different scattering orders are shown in Table 6. When the scattering order increases from 3 to 7, MG results without MHT show a reduction of 105 pcm in the reactivity overestimation. When the MHT is used, the increase of the scattering order reduces the bias by 120 pcm. The residual between the results with MHT and A16P12 discretization also decreases from 74 pcm to 33 pcm. Using larger scattering orders almost does not change the result, but the uncertainty of the scattering matrices becomes larger. This suggests that the residual between MHT and the angle discretization method is due to insufficient expansion order.

Table 6
Reactivity bias of MG results with different scattering orders.

Maximum Order	3	5	7
w/o MHT	1192	1121	1087
A16P12	420	362	341
w/i MHT	494	416	374

MG results with MGXS with different energy structures and geometries are shown in Table 7 to study the spatial and energy homogenization effect. The MG calculation without assembly spatial homogenization using MGXS with MHT shows a 460 pcm bias compared to the reference result. It means that the spatial homogenization at the assembly-level in the benchmark only affects the multiplication factor by 34 pcm. When the number of energy groups increases to 172, there is a 122 pcm decrease in the

Table 7
Multiplication factors with different energy group structures.

Group structure	Core geometry	keff	Δρ (pcm)
24G	Homogeneous	1.03424	494
	Heterogeneous	1.03387	460
70G	Homogeneous	1.03373	447
	Heterogeneous	1.03345	420
172G	Homogeneous	1.03294	372
	Heterogeneous	1.03241	322

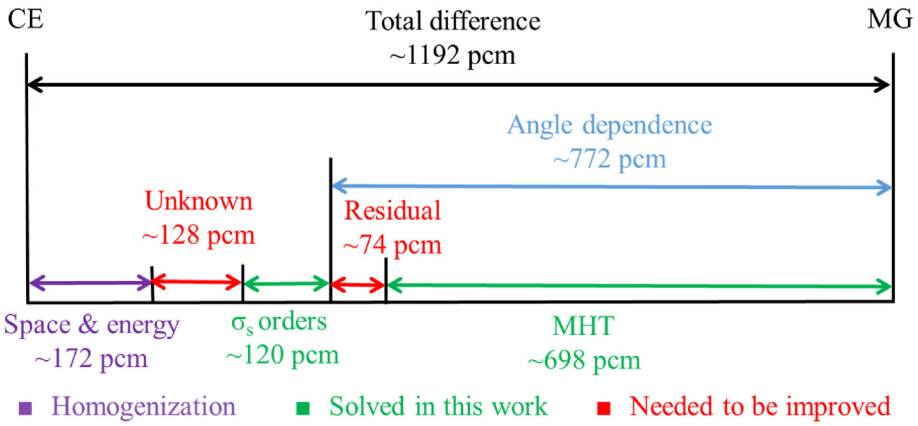

Fig. 7. Decomposition of the reactivity bias between CE and MG results.

reactivity bias. When the heterogeneous structures are retained in the 172-group calculation, the bias is further reduced by 50 pcm. When the number of energy groups is larger than 172, the reactivity bias is almost unchanged with the increase of groups. However, the influence of group structures is not yet studied. This result shows the coupled influence of space and energy homogenization. The effect of spatial and energy homogenization is about 172 pcm.

After excluding the above factors, the reason that causes the remaining 128 pcm bias is unknown at this time. It can contain the effect of inaccurate high-order scattering matrices, the tiny effect from the limited scattering order and broad energy groups, the interaction of the above factors, and elements that could have been neglected in this paper. However, this suggests that the impact of inaccurate high-order scattering matrices is relatively small.

3.6. Summary

The reactivity bias between CE and MG results is shown in Fig. 7. The total difference of MC-MGXS without correction is about 1192 pcm. The angle-dependence of cross-sections contributes a bias of about 772 pcm on this difference. The MHT can catch much of this effect: 698 pcm. The residual 74 pcm come from an insufficient expansion order and the angle-dependence of cross-sections other than Σ_t. The increase of the scattering order contributes to a reduction of about 120 pcm on the reactivity bias, the spatial and energy homogenization leads to a bias of about 172 pcm. The remaining bias of 128 pcm is unknown at this time, inaccurate anisotropic scattering may partly contribute.

4. Conclusion

The Monte-Carlo method can generate accurate multi-group cross-sections because it does not make self-shielding approximations and has the ability to work on arbitrary geometries. The Monte-Carlo generated scalar flux-weighted multi-group cross-sections showed excellent results with diffusion solvers. However, it showed relatively large biases in core calculations with transport solvers. In this paper, the MET-1000 benchmark is used to prove that the bias in MC-MGXS-transport solver is mainly due to the neglect of the angle dependence in the total cross-sections.

Then, a flux-moment homogenization technique is proposed for MGXS generation. The technique takes into account the angle dependence of the total cross-sections in the scattering matrices. The MC-MGXS modified by this technique can compensate well for the influence of the angle dependence of the total cross-sections in OpenMC MG transport solver. It can reduce by 698 pcm the total 774 pcm reactivity bias caused by neglecting the angle-dependence of cross-sections in the benchmark. The reflector regions in the benchmark contribute the most to the angle-dependence effect; the angle-dependent total cross-sections in the structures and in control rod assemblies also lead to obvious biases. The power distribution bias is significantly reduced both at ARO and ARI; the underestimation in the core center and the overestimation in the periphery are reduced due to the higher leakage in reflectors in MGXS with MHT. The factors that cause the residual bias are discussed, but there is only about 130 pcm or unsolved bias with MC-MGXS. The result using MGXS with MHT is close to that with angle-dependent MGXS, and the conciseness and universality of MGXS can be retained. The results show that the modified MC-MGXS is applicable in fast reactor analysis.

However, the combination of MC-MGXS and deterministic code need further investigation. As the cause of the 130 pcm reactivity bias is unknown, the universality of the flux-moment homogenization technique needs to be further verified in depletion simulation, and for other benchmarks. These issues and shortcomings will be addressed in subsequent work.

Declaration of competing interest

The authors declare that they have no known competing financial interests or personal relationships that could have appeared to influence the work reported in this paper.

Acknowledgment

This study is sponsored by the National Natural Science Foundation of China (No. 12105170, 12135008). The computations in this paper were run on the π 2.0 cluster supported by the Center for High-Performance Computing at Shanghai Jiao Tong University.

References

[1] J.E. Hoogenboom, V.A. Khotylev, J.M. Tholammakkil, Generation of multi-group cross sections and scattering matrices with the Monte Carlo code MCNP5, in: J. Gonnord, T. Tajima (Eds.), Proceedings M&C+SNA 2007 Conference, ANS, Monterey, CA, USA, 2007, pp. 1–8, 15-19 April 2007.

[2] J.T. Goorley, M.R. James, T.E. Booth, J.S. Bull, L.J. Cox, J.W. Durkee Jr., J.S. Elson, M.L. Fensin, R.A.I. Forster, J.S. Hendricks, H.G.I. Hughes, R.C. Johns, B.C. Kiedrowski, R.L. Martz, S.G. Mashnik, G.W. McKinney, D.B. Pelowitz, R.E. Prael, J.E. Sweezy, L.S. Waters, T. Wilcox, A.J. Zukaitis, in: Initial MCNP6 Release Overview - MCNP6 Version 1.0, 2013, 1086758, https://doi.org/10.2172/1086758. LA-UR-13-22934.

[3] H.J. Shim, Y.C. Jin, J.S. Song, H.K. Chang, Generation of few group diffusion theory constants by Monte Carlo code, Trans. Am. Nucl. Soc. 99 (2008) 343–345.

[4] H.J. Park, H.J. Shim, H.G. Joo, C.H. Kim, Generation of few-group diffusion theory constants by Monte Carlo code McCARD, Nucl. Sci. Eng. 172 (2012) 66–77, https://doi.org/10.13182/NSE11-22.
[5] J. Leppänen, M. Pusa, E. Fridman, Overview of methodology for spatial homogenization in the Serpent 2 Monte Carlo code, Ann. Nucl. Energy 96 (2016) 126–136, https://doi.org/10.1016/j.anucene.2016.06.007.
[6] E. Fridman, J. Leppänen, On the use of the Serpent Monte Carlo code for few-group cross section generation, Ann. Nucl. Energy 38 (2011) 1399–1405, https://doi.org/10.1016/j.anucene.2011.01.032.
[7] K. Wang, Z. Li, D. She, J. Liang, Q. Xu, Y. Qiu, J. Yu, J. Sun, X. Fan, G. Yu, Rmc – a Monte Carlo code for reactor core analysis, Ann. Nucl. Energy 82 (2015) 121–129, https://doi.org/10.1016/j.anucene.2014.08.048.
[8] W. Boyd, A. Nelson, P.K. Romano, S. Shaner, B. Forget, K. Smith, Multigroup cross-section generation with the OpenMC Monte Carlo particle transport code, Nucl. Technol. 205 (2019) 928–944, https://doi.org/10.1080/00295450.2019.1571828.
[9] T.D.C. Nguyen, H. Lee, D. Lee, Use of Monte Carlo code MCS for multigroup cross section generation for fast reactor analysis, Nucl. Eng. Technol. 53 (2021) 2788–2802, https://doi.org/10.1016/j.net.2021.03.005.
[10] E. Nikitin, E. Fridman, K. Mikityuk, Solution of the OECD/NEA neutronic SFR benchmark with Serpent-DYN3D and Serpent-PARCS code systems, Ann. Nucl. Energy 75 (2015) 492–497, https://doi.org/10.1016/j.anucene.2014.08.054.
[11] N. Martin, R. Stewart, S. Bays, A multiphysics model of the versatile test reactor based on the MOOSE framework, Ann. Nucl. Energy 172 (2022), 109066, https://doi.org/10.1016/j.anucene.2022.109066.
[12] C.-S. Lin, W.S. Yang, An assessment of the applicability of multigroup cross sections generated with Monte Carlo method for fast reactor analysis, Nucl. Eng. Technol. 52 (2020) 2733–2742, https://doi.org/10.1016/j.net.2020.05.029.
[13] H. Guo, Y. Wu, X. Jin, K. Feng, X. Huo, H. Gu, Preliminary verification of multi-group cross-sections generation and locally heterogeneous transport calculation using OpenMC with CEFR start-up tests benchmark, Prog. Nucl. Energy 154 (2022), 104484, https://doi.org/10.1016/j.pnucene.2022.104484.
[14] P.K. Romano, B. Forget, The OpenMC Monte Carlo particle transport code, Ann. Nucl. Energy 51 (2013) 274–281, https://doi.org/10.1016/j.anucene.2012.06.040.
[15] A.G. Nelson, W. Boyd, P.K. Romano, The effect of the flux separability approximation on multigroup neutron transport, JNE 2 (2021) 86–96, https://doi.org/10.3390/jne2010009.
[16] T.Q. Tran, A. Cherezov, X. Du, D. Lee, Verification of a two-step code system MCS/RAST-F to fast reactor core analysis, Nucl. Eng. Technol. (2021), https://doi.org/10.1016/j.net.2021.10.038. S1738573321006227.
[17] J.M. Ruggieri, J. Tommasi, J.F. Lebrat, C. Suteau, D. Plisson-Rieunier, C. De Saint Jean, G. Rimpault, J.C. Sublet, Eranos 2.1 : international code system for GEN IV fast reactor analysis, in: American Nuclear Society - ANS, 2006. La Grange Park (United States), Reno, USA, https://www.osti.gov/biblio/21021146. La Grange Park (United States), Reno, USA.
[18] E. Nikitin, E. Fridman, K. Mikityuk, On the use of the SPH method in nodal diffusion analyses of SFR cores, Ann. Nucl. Energy 85 (2015) 544–551, https://doi.org/10.1016/j.anucene.2015.06.007.
[19] J.-F. Vidal, P. Archier, A. Calloo, P. Jacquet, J. Tommasi, An improved energy-collapsing method for core-reflector modelization in sfr core calculations using the paris platform, in: PHYSOR 2012, Tennessee, Knoxville, 2012, p. 15. USA.
[20] J.-F. Vidal, P. Archier, B. Faure, V. Jouault, J.-M. Palau, V. Pascal, G. Rimpault, F. Auffret, L. Graziano, E. Masiello, S. Santandrea, APOLLO3® homogenization techniques for transport core calculations - application to the ASTRID CFV core, Nucl. Eng. Technol. 49 (2017) 1379–1387, https://doi.org/10.1016/j.net.2017.08.014.
[21] R. Qiu, X. Ma, Q. Xu, J. Liu, Y. Chen, Development and verification of multi-group cross section process code TXMAT for fast reactor RBEC-M analysis, in: Volume 3: Nuclear Fuel and Material, Reactor Physics and Transport Theory; Innovative Nuclear Power Plant Design and New Technology Application, American Society of Mechanical Engineers, Shanghai, China, 2017, V003T02A015, https://doi.org/10.1115/ICONE25-66550.